Dalton Transactions

Cite this: *Dalton Trans.*, 2011, **40**, 5188

www.rsc.org/dalton

PAPER

1-(2-Picolyl)-substituted 1,2,3-triazole as novel chelating ligand for the preparation of ruthenium complexes with potential anticancer activity†

Ioannis Bratsos,*[a] Damijana Urankar,[b] Ennio Zangrando,[a] Petia Genova-Kalou,[c] Janez Košmrlj,[b] Enzo Alessio[a] and Iztok Turel*[b]

Received 22nd December 2010, Accepted 24th February 2011
DOI: 10.1039/c0dt01807d

The 1,4-disubstituted 1,2,3-triazole ligand prepared by click chemistry 1-(2-picolyl)-4-phenyl-1*H*-1,2,3-triazole (**ppt**) was investigated as novel chelating ligand for Ru(II) complexes with potential antitumor activity. The preparation and structural characterization, mainly by NMR spectroscopy in solution and by X-Ray crystallography in the solid state, of four new Ru(II) complexes is reported: two isomeric Ru-dmso compounds, *trans*,*cis*-[$RuCl_2$(dmso-S)$_2$(**ppt**)] (**1**) and *cis*,*cis*-[$RuCl_2$(dmso-S)$_2$(**ppt**)] (**2**), and two half-sandwich Ru-[9]aneS_3 coordination compounds, [Ru([9]aneS_3)(dmso-S)(**ppt**)][CF_3SO_3]$_2$ (**3**) and [Ru([9]aneS_3)Cl(**ppt**)][CF_3SO_3] (**4**). In all compounds **ppt** firmly binds to ruthenium in a bidentate fashion through the pyridyl nitrogen atom and the triazole N2, thus forming a puckered six-membered ring. The chemical behavior in aqueous solution of the water-soluble complexes **3** and **4** was studied by UV-Vis and NMR spectroscopy and compared to that of the previously described organometallic analogue [Ru(η^6-*p*-cymene)Cl(**ppt**)][Cl] (**5**) in view of their potential antitumor activity. Compounds **3–5** were tested also *in vitro* for cytotoxic activity against two human cancer cell lines, one sensitive and one resistant to cisplatin, in comparison with cisplatin. Compound **4**, the one that aquates faster, was found to be more cytotoxic than cisplatin against human lung squamose carcinoma cell line (A-549).

Introduction

In the development of novel non-platinum metal anticancer drugs with improved properties, ruthenium compounds occupy a prominent position,[1,2] especially after the introduction of two Ru(III) coordination compounds, NAMI-A ([imH]*trans*-[$RuCl_4$(dmso-S)(im)], im = imidazole) and KP1019 ([indH]*trans*-[$RuCl_4$(ind)$_2$], ind = indazole), in clinical trials.[3,4] These two complexes display an activity that is markedly different from that of cisplatin and the other established platinum anticancer chemotherapeutics: NAMI-A shows negligible cytotoxicity *in vitro* against cancer cells whereas it is particularly active against the development and growth of pulmonary metastases of solid tumors;[5] KP1019 is moderately cytotoxic *in vitro* but was proved to possess excellent activity against platinum-resistant colorectal tumors in animal models.[6]

In recent years, the focus on ruthenium anticancer drugs has shifted from coordination to organometallic compounds. New classes of half-sandwich Ru(II)-arene compounds were found to have promising anticancer activity.[7] In particular, compounds of the general formula [Ru(η^6-arene)Cl(en)][PF_6] (en = 1,2-diaminoethane), developed by the group of Sadler,[8,9] showed excellent activity both *in vitro* against human cancer cells, including some platinum-resistant lines, and *in vivo* against animal tumor models.[10] Extensive structure–activity relationship (SAR) investigations showed that the anticancer properties of these complexes - that are believed to be activated through hydrolysis of the chlorido ligand and to target DNA - are influenced by the nature of each ligand. In particular, it was found that increasing the size and hydrophobicity of the arene ligand improves the cell uptake and the interaction with DNA and, as a consequence, also the anticancer activity. In addition, the presence of 1,2-diaminoethane as chelating ligand is very important: replacement of en with other *N–N*, *N–O* or *O–O* chelating ligands generally leads to decreased activity.[11]

[a]*Dipartimento di Scienze Chimiche e Farmaceutiche, Università di Trieste, Via L. Giorgieri 1, 34127, Trieste, Italy. E-mail: jbratsos@units.it*
[b]*Faculty of Chemistry and Chemical Technology, University of Ljubljana, Aškerčeva 5, Ljubljana, Slovenia. E-mail: Iztok.Turel@fkkt.uni-lj.si*
[c]*Department of Virology, Laboratory of Herpesvirus Infections and Cell Cultures, National Centre of Infectious and Parasitic Diseases, 44A Stoletov Street, 1233, Sofia, Bulgaria*

† Electronic supplementary information (ESI) available: Tables of X-ray crystallographic data in CIF format for compounds **1–4**; Crystal packing of **1**; ^{1}H NMR spectra of **1** and **2** in $CDCl_3$; 2D homonuclear ^{1}H-^{1}H COSY and heteronuclear ^{1}H-^{13}C HSQC NMR spectra of **1** in $CDCl_3$; ^{1}H NMR spectra of **3** and **4** in CD_3NO_2; ^{1}H-^{1}H COSY NMR spectrum of **3** in CD_3NO_2; 2D heteronuclear ^{1}H-^{13}C HSQC and HMBC NMR spectra of **3** in CD_3NO_2; 2D homonuclear ^{1}H-^{1}H COSY and heteronuclear ^{1}H-^{13}C HSQC NMR spectrum of **4** in CD_3NO_2; ^{1}H NMR spectral changes during the aquation of **4** in D_2O at 25.0 °C; ^{1}H NMR spectral changes upon addition of 100mM NaCl to equilibrated solution of **4** and **3a** in D_2O at 25.0 °C; ^{1}H NMR spectral changes during the aquation of **5** in D_2O; Time evolution of UV-Vis spectra (of **3–5**) and UV-Vis difference spectra (of **4** and **5**) in H_2O at 25.0 °C; Tables with assignments of ^{1}H and ^{13}C resonances (δ) for complexes **1–5** in various solvents and for aquation products **3a** and **5a**. CCDC reference numbers 805600–805603. For ESI and crystallographic data in CIF or other electronic format see DOI: 10.1039/c0dt01807d

Intrigued by these results, we reasoned that perhaps the η^6-arene fragment of these anticancer half-sandwich organometallic compounds might be effectively replaced by another neutral 6-electron donor face-capping ligand, while maintaining the other ligands unchanged. Thus, we developed series of new half-sandwich Ru(II) *coordination compounds* of the general formula [Ru([9]aneS$_3$)Cl(*N*–*N*)][CF$_3$SO$_3$], [Ru([9]aneS$_3$)(dmso-S)(*N*–*N*)][CF$_3$SO$_3$]$_2$,[12,13] [Ru([9]aneS$_3$)(dmso-S)(*O*–*O*)],[14] and [Ru([9]aneN$_3$)(dmso-S)(*N*–*N*)][PF$_6$]$_2$[15] (where *N*–*N* = nitrogen chelating ligand such as en, bpy or substituted bpy; *O*–*O* = chelating dicarboxylate ligand such as oxalate or malonate) in which the aromatic fragment was replaced either by the tridentate sulfur macrocycle 1,4,7-trithiacyclononane ([9]aneS$_3$) or by the corresponding nitrogen macrocycle 1,4,7-triazacyclononane ([9]aneN$_3$). *In vitro* experiments on selected complexes showed that only the half-sandwich complex [Ru([9]aneS$_3$)Cl(en)][CF$_3$SO$_3$] has a moderate cytotoxicity against human and murine cancer cell lines (IC$_{50}$ values in the range from 65 to 175 μM), which is *ca.* one order of magnitude lower than that of [Ru(η^6-bip)Cl(en)][PF$_6$] (bip = biphenyl), *i.e.* the most cytotoxic among the Ru-arene analogues, against the same cell lines.[12,13] Thus, it emerged that selected Ru(II)-[9]aneS$_3$ half-sandwich coordination compounds can have a reasonable antiproliferative activity *in vitro* against cancer cell lines and, above all, that the nature of the chelating ligand is more important than that of the face-capping ligand for determining such activity. More recently, we also reported that the conjugation of Ru(II)-[9]aneS$_3$ half-sandwich compounds to porphyrins leads to enhanced cytotoxicity (in the low micromolar range), which is further improved upon irradiation with visible light (photo-toxicity).[16]

Now, with the aim of expanding the SAR investigation on these half-sandwich coordination compounds, we are testing other face-capping and chelating ligands. In this context, we were intrigued by the possibility of using 1-(2-picolyl)-substituted 1,2,3-triazoles as a new class of versatile neutral *N*-*N* chelators whose physico-chemical properties can be easily varied.

1,4-Disubstituted 1,2,3-triazoles are actively investigated in diverse areas of chemistry - such as dendrimers, polymers, catalysis, drug discovery, materials science and bioconjugation - as ready-to-make linkers between two functional groups.[17] By virtue of their facile and versatile synthetic procedure - the copper(I)-catalyzed alkyne-azide cycloaddition, known also as "click chemistry"[18,19] - the nature of the functional groups at positions 1 and 4 can be varied almost at will within a wide range.

In coordination chemistry, appropriately designed 1,4-disubstituted 1,2,3-triazoles can behave as monodentate ligands or as chelators towards metal ions, depending on the nature of the substituents. Bidentate chelation can occur when one of the substituents bears an appropriate donor atom; in this case, coordination of the triazole group can involve either the N3 or N2 atom (chelator **A** and **B**, respectively, in Fig. 1), depending on the position and nature of the pendant coordinating group. Owing to distinct Lewis basicity of N3 and N2,[20] the complexes arising from these two binding modes can differ greatly in stability. Conveniently, the stability can be finely tuned by the appropriate selection of the pendant coordinating group.[21–24] Recent reports demonstrated that when a 2-picolyl group is linked at the N1 atom the molecule behaves as a highly efficient bidentate ligand through the triazole N2 and the pyridyl nitrogen atom, *i.e.* as chelator

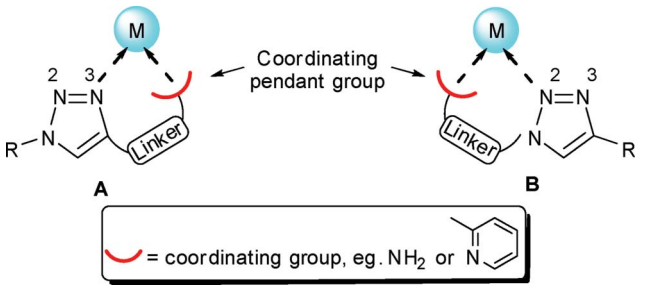

Fig. 1 Schematic representation of the two isomeric 1,4-disubstituted 1,2,3-triazole chelators **A** and **B**.

of type **B**.[24–31] Thus 1-(2-picolyl)-4-phenyl-1*H*-1,2,3-triazole (**ppt**) was proved to bind in this fashion a variety of metal ions, such as Co^{II}, Ni^{II}, Cu^{II}, Zn^{I}, Ru^{II}, Pd^{II}, Ag^{I}, Pt^{II} and Hg^{II}, forming stable 6-membered chelate rings. Very recently it was proved that **ppt**, having three potential coordination sites (*i.e.* N2 and N3 of the triazole and the N pyridyl atom) can adopt also other binding modes including monodentate and bridging bidentate, depending on the metal center and the experimental conditions.[32]

In this work, we first investigated the reactivity of **ppt** towards two common Ru(II)-dmso precursors, namely *trans*-[RuCl$_2$(dmso-S)$_4$] and *cis*,*fac*-[RuCl$_2$(dmso-S)$_3$(dmso-O)] (from now on simply *trans*-[RuCl$_2$(dmso)$_4$] (**P1**) and *cis*-[RuCl$_2$(dmso)$_4$] (**P2**), respectively), and isolated two new isomeric compounds *trans*,*cis*-[RuCl$_2$(dmso-S)$_2$(**ppt**)] (**1**), and *cis*,*cis*-[RuCl$_2$(dmso-S)$_2$(**ppt**)] (**2**), respectively (Fig. 2). Then, with the aim of evaluating the potential use of **ppt** as chelating ligand in Ru-[9]aneS$_3$ compounds and its influence on *in vitro* anticancer activity we prepared the two new half-sandwich complexes [Ru([9]aneS$_3$)(dmso-S)(**ppt**)][CF$_3$SO$_3$]$_2$ (**3**) and [Ru([9]aneS$_3$)Cl(**ppt**)][CF$_3$SO$_3$] (**4**) (Fig. 2). In all compounds **ppt** behaves as a chelating ligand through the triazole N2 and the pyridyl N. The chemical behavior of the water soluble complexes **3** and **4**, and of the previously described organometallic analogue [Ru(η^6-*p*-cymene)Cl(**ppt**)][Cl] (**5**),[24] were studied in aqueous solution by ^{1}H NMR spectroscopy, whereas their aquation kinetics were investigated by UV-Vis spectroscopy. We report also the results of *in vitro* cytotoxicity tests performed on complexes **3**–**5** against two human cancer cell lines (human larynx carcinoma cell line (HEp-2), and human alveolar squamous carcinoma epithelial cells (A-549)) in comparison with their respective precursors, with the free ligand **ppt** and with cisplatin.

Experimental

Materials

The compound [RuCl(η^6-*p*-cymene)(**ppt**)][Cl] (**5**),[24] the precursors *trans*-[RuCl$_2$(dmso)$_4$] (**P1**),[33] *cis*-[RuCl$_2$(dmso)$_4$] (**P2**),[33] [Ru([9]-aneS$_3$)(dmso)$_3$][CF$_3$SO$_3$]$_2$ (**P3**),[34] and [Ru([9]aneS$_3$)Cl(dmso-S)$_2$][CF$_3$SO$_3$] (**P4**)[34] and the ligand 1-(2-picolyl)-4-phenyl-1*H*-1,2,3-triazole (**ppt**),[24] were synthesized according to published procedures. The compounds [RuCl(μ-Cl)(η^6-*p*-cymene)]$_2$ (**P5**) and *cis*-[PtCl$_2$(NH$_3$)$_2$] (cisplatin) were purchased from Sigma-Aldrich. All other chemicals were used as purchased without further purification.

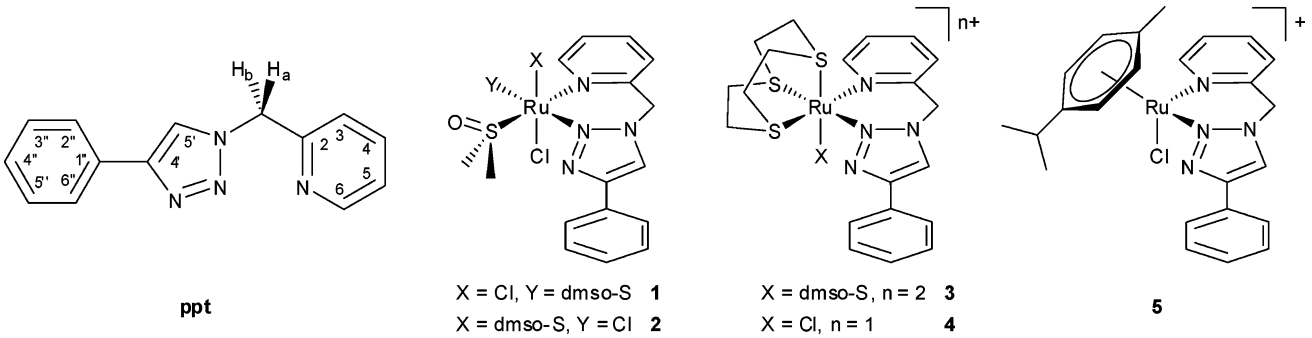

Fig. 2 Schematic structures of the ligand 1-(2-picolyl)-4-phenyl-1*H*-1,2,3-triazole (**ppt**) with numbering scheme used for the NMR characterization, of the new ruthenium complexes *trans*,*cis*-[$RuCl_2$(dmso-S)$_2$(**ppt**)] (**1**), *cis*,*cis*-[$RuCl_2$(dmso-S)$_2$(**ppt**)] (**2**), [Ru([9]aneS_3)(dmso-S)(**ppt**)][CF_3SO_3]$_2$ (**3**) and [Ru([9]aneS_3)Cl(**ppt**)][CF_3SO_3] (**4**), and of the organometallic analogue [Ru(η^6-*p*-cymene)Cl(**ppt**)][Cl] (**5**).

Instrumental Methods

Mono- (^{1}H (400 or 500 MHz), ^{13}C (100.5 MHz)) and bi-dimensional (^{1}H-^{1}H COSY, ^{1}H-^{13}C HSQC, ^{1}H-^{13}C HMBC) NMR spectra were recorded on a JEOL Eclipse 400FT or on a Varian 500 spectrometer. ^{1}H chemical shifts in D_2O were referenced to the internal standard 2,2-dimethyl-2,2-silapentane-5-sulfonate (DSS) at δ = 0.00, while in other solvents were referenced to the peak of residual non-deuterated solvent (δ = 7.26 for $CDCl_3$, 4.33 for CD_3NO_2); ^{13}C chemical shifts were referenced to the peak of residual non-deuterated solvent (δ = 77.2 for $CDCl_3$, 62.8 for CD_3NO_2). NMR aquation studies were performed on 2.0 mM samples of complexes **3–5** in D_2O at 25.0 °C. Assignments of ^{1}H and ^{13}C resonances (δ) of complexes **1–5** in various solvents and of aquation products are summarized in ESI† (Tables S1 and S2). UV-Vis spectra were obtained on a Jasco V-500 UV-Vis spectrophotometer equipped with a Peltier temperature controller, using 1.0 cm path-length quartz cuvettes (3.0 mL). Infrared spectra (ATR) were recorded on a Perkin-Elmer Spectrum 100 spectrometer (wavelength range: 4000 to 600 cm^{-1}). Elemental analysis was performed at the Department of Chemistry, University of Udine (Italy).

Synthesis of the complexes

***trans*,*cis*-[$RuCl_2$(dmso-S)$_2$(ppt)] (1).** Equimolar amounts of **P1** (100.0 mg, 0.206 mmol) and **ppt** (48.7 mg, 0.206 mmol) were suspended in 5 mL of H_2O and the mixture was vigorously stirred for 24 h at room temperature. During this time, compound **1** precipitated as a yellow solid, and was collected by filtration, washed with H_2O and vacuum dried. (93.9 mg, 81%). Found: C, 38.6; H, 4.31; N, 9.96. $C_{18}H_{24}Cl_2N_4O_2RuS_2$ (564.50) requires: C, 38.3; H, 4.29; N, 9.92. Crystals suitable for X-ray analysis formed spontaneously from the reaction mixture in the absence of stirring. Complex **1** is insoluble in water, while it is soluble in acetone, chloroform, dichloromethane and nitromethane, and slightly soluble in methanol and ethanol. Selected IR ν_{max}/cm^{-1} 3117w, 3086w, 3061w, 1609m, 1486m, 1468m, 1438w, 1412m, 1089s, 763s, 722s and 693s (**ppt**) and 1069vs (S═$O_{(dmso\text{-}S)}$). δ_H (500 MHz, $CDCl_3$) 9.67 (1 H, dd, *J* 5.8, 1.2, C6*H*), 8.11 (1 H, s, C5′*H*), 7.92–7.64 (4 H, m, C4*H*/C*H*^{a}/C2″*H*/C6″*H*), 7.48–7.31 (5 H, m, C3″*H*/C5″*H*/C4″*H*/C5*H*/C3*H*), 5.26 (1 H, br d, C*H*^{b}), 3.86 (3 H, br s, CH_3 dmso-S), 3.64 (3 H, br s, CH_3 dmso-S), 3.52 (3 H, br s, CH_3 dmso-S), 3.19 (3 H, br s, CH_3 dmso-S). δ_H (500 MHz, CD_3NO_2) 9.56 (1 H, dd, *J* 5.9, 1.1 Hz, C6*H*), 8.56 (1 H, s, C5′*H*), 7.97 (1 H, td, *J* 7.6, 1.6, C4*H*), 7.87 (2 H, d, *J* 7.1, C2″*H*/C6″*H*), 7.65 (1 H, d, *J* 7.6, C3*H*), 7.59 (1 H, br d, C*H*^{a}), 7.53–7.40 (4 H, m, C3″*H*/C5″*H*/C5*H*/C4″*H*), 5.69 (1 H, br d, C*H*^{b}), 3.78 (3 H, br s, CH_3 dmso-S), 3.52 (3 H, br s, CH_3 dmso-S), 3.37 (3 H, br s, CH_3 dmso-S), 3.17 (3 H, br s, CH_3 dmso-S). δ_C (101 MHz, $CDCl_3$) 161.4 (*C*6H), 153.9 (*C*2), 149.3 (*C*4′), 138.4 (*C*4H), 129.5 (*C*4″H), 129.3 (*C*3″H/*C*5″H), 128.8 (*C*1″), 125.8 (*C*2″H/*C*6″H), 124.7 (*C*5′H), 124.2 (*C*5H), 124.0 (*C*3H), 56.3 (*C*H$_2$ **ppt**), 46.5 (br, *C*H$_3$ dmso-S), 44.6 (br, *C*H$_3$ dmso-S), 44.2 (br, *C*H$_3$ dmso-S), 43.7 (br, *C*H$_3$ dmso-S). δ_C (101 MHz, CD_3NO_2) 161.8 (*C*6H), 156.3 (*C*2), 149.9 (*C*4′), 140.1 (*C*4H), 130.4 (*C*3″H/*C*5″H), 130.3 (*C*4″H), 126.9 (*C*5′H), 126.8 (*C*2″H/*C*6″H), 126.7 (*C*1″), 125.9 (*C*3H), 124.5 (*C*5H), 56.7 (*C*H$_2$ **ppt**), 46.4 (br, *C*H$_3$ dmso-S), 44.6 (br, *C*H$_3$ dmso-S), 44.5 (br, *C*H$_3$ dmso-S), 43.8 (br, *C*H$_3$ dmso-S).

***cis*,*cis*-[$RuCl_2$(dmso-S)$_2$(ppt)] (2).** A 14.6 mg amount of **ppt** (0.062 mmol) and a 30.0 mg amount of **P2** (0.062 mmol) were partially dissolved in 5 mL of ethanol and the mixture was refluxed for 2 h. During this time the solution—obtained upon warming—turned from yellow to orange and then, after *ca.* 1 h, the formation of the product as yellow solid was observed. After cooling, the product was collected by filtration, washed with ethanol and diethyl ether and vacuum dried (29.7 mg, 85%). Found: C, 38.0; H, 4.17; N, 9.74. $C_{18}H_{24}Cl_2N_4O_2RuS_2$ (564.50) requires: C, 38.3; H, 4.29; N, 9.92. Slow evaporation of the orange filtrate gave rise to the formation of additional product as orange crystals suitable for X-ray analysis. Complex **2** is insoluble in water, ethanol and acetone, while it is soluble in chloroform, dichloromethane and nitromethane, and slightly soluble in methanol. Selected IR ν_{max}/cm^{-1} 3116w, 3089w, 2998w, 1610m, 1484m, 1473m, 1422w, 1089s, 767vs, 717m and 694vs (**ppt**), 1106s and 1082vs (S═$O_{(dmso\text{-}S)}$). δ_H (500 MHz, $CDCl_3$) 9.90 (1 H, d, *J* 5.8, C6*H*), 8.16 (1 H, s, C5′*H*), 7.83 (1 H, t, *J* 7.5, C4*H*), 7.78 (2 H, d, *J* 7.6, C2″*H*/C6″*H*), 7.52–7.36 (6 H, m, C3″*H*/C5″*H*/C4″*H*/C*H*^{a}/C5*H*/C3*H*), 5.41 (1 H, d, *J* 14.9, C*H*^{b}), 3.59 (3 H, s, CH_3 dmso-S), 3.56 (3 H, s, CH_3 dmso-S), 3.35 (3 H, s, CH_3 dmso-S), 3.28 (3 H, s, CH_3 dmso-S). δ_H (500 MHz, CD_3NO_2) 9.74 (1 H, d, *J* 5.7, C6*H*), 8.58 (1 H, s, C5′*H*), 8.02 (1 H, t, *J* 7.0, C4*H*), 7.92 (2 H, d, *J* 7.5, C2″*H*/C6″*H*), 7.67 (1 H, d, *J* 7.3, C3*H*), 7.56–7.48 (3 H, m, C3″*H*/C5″*H*/C5*H*), 7.45 (1 H, t, *J* 7.3, C4″*H*), 7.01 (1 H, d, *J* 15.3, C*H*^{a}), 5.87 (1 H, d, *J* 15.3, C*H*^{b}), 3.41 (3 H, s, CH_3 dmso-S), 3.41 (3 H, s, CH_3

dmso-S), 3.40 (3 H, s, CH_3 dmso-S), 3.19 (3 H, s, CH_3 dmso-S). δ_C (101 MHz, $CDCl_3$) 159.9 (*C*6H), 151.8 (*C*2), 148.8 (*C*4′), 138.6 (*C*4H), 129.8 (*C*4″H), 129.5 (*C*3″H/*C*5″H), 128.4 (*C*1″), 125.6 (*C*2″H/*C*6″H), 125.1 (*C*5′H), 124.3 (*C*5H), 124.1 (*C*3H), 56.1 (*C*H_2 **ppt**), 45.9 (*C*H_3 dmso-S), 45.8 (*C*H_3 dmso-S), 45.3 (*C*H_3 dmso-S), 44.5 (*C*H_3 dmso-S).

[Ru([9]aneS$_3$)(dmso-S)(ppt)][CF$_3$SO$_3$]$_2$ (3). Equimolar amounts of **P3** (50.0 mg, 0.0614 mmol) and of **ppt** (14.5 mg, 0.0614 mmol) were partially dissolved in 5 mL of methanol and the mixture was refluxed for 2h. During this time a yellow solution was obtained. Rotary evaporation to dryness afforded a pale yellow oil that was dissolved in acetone (*ca.* 4 mL). Within 1 day at ambient temperature the product precipitated as white crystals (plates) suitable for X-ray analysis that were collected by filtration, washed with cold acetone and diethyl ether and vacuum dried (41.0 mg, 76%). Found: C, 31.9; H, 3.28; N, 6.12. $C_{24}H_{30}F_6N_4O_7RuS_6$ (893.95) requires: C, 32.2; H, 3.38; N, 6.27. Complex **3** is soluble in water, methanol and nitromethane, slightly soluble in acetone, and insoluble in ethanol, chloroform and dichloromethane. UV-Vis λ_{max} (H_2O)/nm 270 and 289 (ε/dm^3 mol^{-1} cm^{-1} 12 951 and 10 688). Selected IR ν_{max}/cm^{-1} 3151w, 3017w, 2933w, 1610w, 1486m, 1446m, 1429m, 1271s, 1086m, 775m, 753m, 726m and 683m (**ppt**), 1256vs and 1028vs (SO_3), 1223s and 1140s (CF_3), 1099m (S═O$_{(dmso\text{-}S)}$). δ_H (500 MHz, D_2O) 9.34 (1 H, d, *J* 5.5, C6*H*), 8.83 (1 H, s, C5′*H*), 8.23 (1 H, t, *J* 7.7, C4*H*), 7.95 (1 H, d, *J* 7.7, C3*H*), 7.89 (2 H, d, *J* 6.6, C2″*H*/C6″*H*), 7.74 (1 H, t, *J* 6.4, C5*H*), 7.54 (3 H, m, C3″*H*/C4″*H*/C5″*H*), 6.32 (1 H, d, *J* 16.6, C*H*^{a} **ppt**), 6.11 (1 H, d, *J* 16.6, C*H*^{b} **ppt**), 3.65–3.25 (6 H, m, CH_2 [9]aneS$_3$), 3.54 (3 H, s, CH_3 dmso-S), 2.95–2.80 (1 H, m, CH_2 [9]aneS$_3$), 2.70–2.40 (5 H, m, CH_2 [9]aneS$_3$), 1.99 (3 H, s, CH_3 dmso-S). δ_H (500 MHz, CD_3NO_2) 9.48 (1 H, d, *J* 5.2, C6*H*), 8.76 (1 H, s, C5′*H*), 8.26 (1 H, t, *J* 7.7, C4*H*), 7.99 (1 H, d, *J* 7.5, C3*H*), 7.88 (2 H, d, *J* 6.9, C2″*H*/C6″*H*), 7.79 (1 H, t, *J* 6.3, C5*H*), 7.59–7.42 (3 H, m, C3″*H*/C4″*H*/C5″*H*), 6.42 (1 H, d, *J* 16.5, C*H*^{a} **ppt**), 6.16 (1 H, d, *J* 16.5, C*H*^{b} **ppt**), 3.73 (1 H, dd, *J* 14.0, 4.2, CH_2 [9]aneS$_3$), 3.65–3.49 (6 H, m, CH_2 [9]aneS$_3$), 3.57 (3 H, s, CH_3 dmso-S), 3.42 (2 H, dd, *J* 27.1, 9.5, CH_2 [9]aneS$_3$), 2.93 (1 H, td, *J* 14.0, 6.0, CH_2 [9]aneS$_3$), 2.65 (1 H, td, *J* 14.0, 6.0, CH_2 [9]aneS$_3$), 2.53 (4 H, dd, *J* 22.4, 9.5, CH_2 [9]aneS$_3$), 1.88 (3 H, s, CH_3 dmso-S). δ_C (101 MHz, CD_3NO_2) 158.2 (*C*6H), 154.6 (*C*2), 152.0 (*C*4′), 142.6 (*C*4H), 131.1 (*C*4″H), 130.6 (*C*3″H/*C*5″H), 130.5 (*C*3H), 129.6 (*C*1″), 129.1 (*C*5′H), 128.8 (*C*5H), 127.1 (*C*2″H/*C*6″H), 56.0 (*C*H_2 **ppt**), 47.2 (*C*H_3 dmso-S), 43.1 (*C*H_3 dmso-S), 38.4 (*C*H_2 [9]aneS$_3$), 38.3 (*C*H_2 [9]aneS$_3$), 38.0 (*C*H_2 [9]aneS$_3$), 31.1 (*C*H_2 [9]aneS$_3$), 30.0 (*C*H_2 [9]aneS$_3$), 29.5 (*C*H_2 [9]aneS$_3$).

[Ru([9]aneS$_3$)Cl(ppt)][CF$_3$SO$_3$] (4). Equimolar amounts of **ppt** (19.0 mg, 0.0803 mmol) and of the precursor **P4** (50.0 mg, 0.0803 mmol) were partially dissolved in 5 mL of methanol and the reaction mixture was refluxed for 3h. During this time a yellow solution was obtained. Rotary concentration to half volume and saturation by diethyl ether led, within 1 day, to the formation of the product as a yellow solid that was collected by filtration, washed with cold acetone and diethyl ether and vacuum dried (43.2 mg, 77%). Found: C, 35.5; H, 3.44; N, 7.84. $C_{21}H_{26}ClF_3N_4O_4RuS_4$ (702.22) requires: C, 35.9; H, 3.44; N, 7.98. Crystals suitable for X-ray analysis were obtained by slow diffusion of diethyl ether into a solution of **4** in methanol. Complex **4** is soluble in water, methanol, acetone, dichloromethane and nitromethane while is slightly soluble in ethanol and chloroform. UV-Vis λ_{max} (H_2O)/nm 248sh, 281, 293 and 400 (ε/dm^3 mol^{-1} cm^{-1} 9 796, 7 391, 7 237 and 815). Selected IR ν_{max}/cm^{-1} 3120w, 3089w, 2979w, 1603w, 1474m, 1446m, 1437m, 1415m, 1270vs, 1089m, 766vs, 755m, 723m and 696s (**ppt**), 1253vs and 1027vs (SO_3), 1223s and 1140s (CF_3). δ_H (500 MHz, D_2O) 9.27 (1 H, d, *J* 5.2, C6*H*), 8.62 (1 H, s, C5′*H*), 8.01 (1 H, t, *J* 7.7, C4*H*), 7.84 (2 H, d, *J* 7.1, C2″*H*/C6″*H*), 7.74 (1 H, d, *J* 7.6, C3*H*), 7.53 (3 H, t, *J* 7.6, C3″*H*/C4″*H*/C5″*H*), 7.49 (1 H, m, *J* 7.1, C5*H*), 6.36 (1 H, d, *J* 16.0, C*H*^{a} **ppt**), 5.94 (1 H, d, *J* 16.0, C*H*^{b} **ppt**), 3.20–3.11 (1 H, m, CH_2 [9]aneS$_3$), 2.96 (2 H, t, *J* 6.5, CH_2 [9]aneS$_3$), 2.87–2.42 (9 H, m, CH_2 [9]aneS$_3$). δ_H (500 MHz, CD_3NO_2) 9.24 (1 H, d, *J* 5.3, C6*H*), 8.52 (1 H, s, C5′*H*), 8.02 (1 H, t, *J* 7.4, C4*H*), 7.85 (2 H, d, *J* 7.4, C2″*H*/C6″*H*), 7.74 (1 H, d, *J* 7.6 Hz, C3*H*), 7.60–7.38 (4 H, m, C5*H*/C3″*H*/C4″*H*/C5″*H*), 6.28 (1 H, d, *J* 15.7, C*H*^{a} **ppt**), 6.10 (1 H, d, *J* 15.7, C*H*^{b} **ppt**), 3.29–3.21 (1 H, m, CH_2 [9]aneS$_3$), 3.10–2.90 (5 H, m, CH_2 [9]aneS$_3$), 2.88–2.80 (1 H, m, CH_2 [9]aneS$_3$), 2.71–2.62 (1 H, m, CH_2 [9]aneS$_3$), 2.59–2.50 (1 H, m, CH_2 [9]aneS$_3$), 2.50–2.38 (3 H, m, CH_2 [9]aneS$_3$). δ_C (101 MHz, CD_3NO_2) 158.4 (*C*6H), 155.1 (*C*2), 150.2 (*C*4′), 140.2 (*C*4H), 130.7 (*C*1″), 130.5 (*C*3″H/*C*5″H), 130.4 (*C*4″H), 127.7 (*C*3H), 127.0 (*C*2″H/*C*6″H), 126.8 (*C*5H), 126.6 (*C*5′H), 56.0 (*C*H_2 **ppt**), 37.9 (*C*H_2 [9]aneS$_3$), 35.1 (*C*H_2 [9]aneS$_3$), 34.9 (*C*H_2 [9]aneS$_3$), 34.8 (*C*H_2 [9]aneS$_3$), 31.7 (*C*H_2 [9]aneS$_3$), 31.4 (*C*H_2 [9]aneS$_3$).

[Ru(η^6-*p*-cymene)Cl(ppt)][Cl] (5). The preparation and the NMR characterization (either in $CDCl_3$ as Cl salt or in DMF-d_7 as CF_3SO_3 salt) have been previously reported.[24] Herein, we report the UV-Vis spectrum in H_2O and the assignment of its ^{1}H NMR spectrum in D_2O, which are relevant for the current experiments. UV-Vis λ_{max} (H_2O)/nm 246, 267 sh, 286 sh and 401 (ε/dm^3 mol^{-1} cm^{-1} 10 788, 8 991, 5 143 and 415). δ_H (500 MHz, D_2O) 9.06 (1 H, d, *J* 4.6, C6*H*), 8.72 (1 H, s, C5′*H*), 8.11 (1 H, t, *J* 7.2, C4*H*), 7.94–7.72 (3 H, m, C2″*H*/C6″*H*/C3*H*), 7.65 (1 H, t, *J* 5.5, C5*H*), 7.58–7.45 (3 H, m, C3″*H*/C5″*H*/C4″*H*), 6.17–6.08 (2 H, m, C*H*^{a}/C*H* Ar), 6.05 (1 H, d, *J* 5.2, C*H* Ar), 5.92 (2 H, t, *J* 5.9, 2×C*H* Ar), 5.68 (1 H, d, *J* 15.5, C*H*^{b}), 2.94–2.83 (1 H, m, CH$_3$C*H* Ar), 2.08 (3 H, s, CH_3 Ar), 1.28 (6 H, t, *J* 7.7, 2×CH_3CH Ar).

Crystallographic Measurements

Data collection for crystal structure analysis of **1–4** was carried out at room temperature on an Enraf Nonius DIP1030H single crystal diffractometer (Mo-Kα radiation, $\lambda = 0.71073$ Å). Cell refinement, indexing and scaling of all the data sets were performed using programs Denzo and Scalepack.[35] The structures were solved by direct methods and subsequent Fourier analyses[36] and refined by the full-matrix least-squares method based on F^2 with all observed reflections.[36] Hydrogen atoms were placed at calculated positions. The structural determination of compound **3** evidenced a triflate anion ($CF_3SO_3^-$) highly disordered that was refined with isotropic atoms and restrains on its geometry. Consequently the final *R* values are higher than those obtained for other compounds (Table 1). In **4** the ΔFourier map evidenced a residual interpreted as a water oxygen (H atoms not located). All the calculations were performed using the WinGX System, Ver 1.80.05.[37] Crystal data and details of data collections and refinements for the structures reported are summarized in Table 1.

Table 1 Crystallographic data for compounds **1–4**

	1	**2**	**3**	**4**·H_2O
Empirical formula	$C_{18}H_{24}Cl_2N_4O_2RuS_2$	$C_{18}H_{24}Cl_2N_4O_2RuS_2$	$C_{24}H_{30}F_6N_4O_7RuS_6$	$C_{21}H_{26}ClF_3N_4O_4RuS_4$
fw	564.50	564.50	893.95	720.22
Crystal system	Triclinic	Monoclinic	Triclinic	Triclinic
Space group	$P\bar{1}$	$P2_1/c$	$P\bar{1}$	$P\bar{1}$
a/Å	8.411(3)	10.796(3)	12.590(3)	8.276(3)
b/Å	10.009(4)	12.813(3)	12.611(3)	13.690(4)
c/Å	13.997(4)	16.220(4)	12.511(5)	14.262(4)
α (°)	104.37(3)		64.09(2)	86.21(3)
β (°)	96.23(2)	91.19(2)	71.65(3)	73.46(2)
γ (°)	94.18(2)		85.07(3)	71.34(2)
V/Å^3	1128.6(7)	2243.2(10)	1692.7(9)	1467.0(8)
Z	2	4	2	2
D_{calcd}/g cm^{-3}	1.661	1.671	1.754	1.630
μ(Mo-Kα)/mm^{-1}	1.139	1.146	0.915	0.963
F(000)	572	1144	904	728
θ range, deg	2.26–27.08	3.42–28.73	1.71–26.37	2.67–27.08
no. of reflns collcd	13115	14079	15655	21726
no. of indep reflns	4678	5423	6379	5825
R_{int}	0.0397	0.0754	0.0516	0.0351
no. of reflns ($I > 2\sigma(I)$)	2373	2541	3177	2755
no. of refined params	266	267	398	343
goodness-of-fit (F^2)	0.839	0.838	0.911	0.860
R_1, wR_2 ($I > 2\sigma(I)$)[a]	0.0421, 0.0960	0.0460, 0.1027	0.0763, 0.1980	0.0598, 0.1655
residuals/e Å^{-3}	0.503, –0.653	0.813, –0.493	1.097, –0.897	0.760, –0.472

[a] $R1 = \Sigma \; ||Fo| - |Fc|| / \Sigma \, |Fo|$, $wR2 = [\Sigma \; w \, (Fo^2 - Fc^2)^2 / \Sigma w \, (Fo^2)^2]^{\frac{1}{2}}$.

Aquation Kinetics

The aquation kinetics of the water soluble complexes **3–5** were studied by UV-Vis spectroscopy (0.15 mM samples in distilled H_2O) at 25.0 °C. For each complex the wavelength selected for the kinetic studies corresponded to that of the maximum change in absorption (derived from the difference spectra). The absorbance at the selected wavelength was recorded at 60 s intervals and the absorption/time data for each complex were computer-fitted, using the program Microcal Origin 5.0, to the first-order rate equation (eqn (1)), which gave the k_{H_2O} value (k) for each aquation process

$$A = C_0 + C_1 e^{-kt} \quad (1)$$

C_0 and C_1 are computer-fitted constants, and A is the absorbance corresponding to time t.

In vitro Studies

Tested Compounds and Precursors. The two new water-soluble coordination half-sandwich complexes **3** and **4** and the organometallic analog **5** were selected for *in vitro* tests in comparison with their precursors **P3** and **P5**, with the free ligand **ppt** and with cisplatin.

The compounds under study were first dissolved in PBS (pH 7.4) to a concentration of 1000 μM and then diluted in cell growth medium with 2% fetal bovine serum. Eight dilutions of each compound and precursor (800 μM maximum concentration) were prepared and immediately tested, with incubation periods of 48 h or 72 h.

Cell lines. Human larynx carcinoma cell line (HEp-2) and human alveolar squamous carcinoma epithelial cells (A-549) were grown as monolayer culture in DMEM supplemented with 5% to 10% fetal bovine serum (FBS), 50 mU/ml penicillin and 50 μg ml^{-1} streptomycin. The culture was maintained at 37.0 °C in a humidified CO_2 incubator. For routine passages monolayers were detached using a mixture of 0.05% trypsin (Gibco)/0.02% ethylendiamino tetraacetic (EDTA).

Method for determining IC_{50}. Cells were seeded into 96-well tissue culture plates (Grainer) at a concentration of 2 × 10^4 cells/well and cultured at 37.0 °C in a CO_2 atmosphere. On the 24 h cells from confluent monolayers were washed and covered with media containing the compounds tested in concentrations 0.001 μM, 0.01 μM, 0.1 μM, 1 μM, 10 μM, 100 μM, 250 μM, 500 μM and 800 μM. Cells grown in compound-free medium served as a control. After 48 h and 72 h the viability of cells was read by microscopy of unstained cell monolayers and by the MTT-assay.[38] MTT, a tetrazolium dye [3-(4,5-dimethyldiazol-2-yl)-2,5 diphenyl tetrazolium bromide; Thiazolyl blue] (Sigma) was added to each well in the assay in a volume of 10 μl at a concentration of 5 mg ml^{-1}. Plates were incubated in the presence of MTT dye for 3 h. Mitochondrial dehydrogenase activity reduces the yellow MTT dye to a purple formazan, which is then solubilized with DMSO:ethanol (1 : 1), and absorbance was read at 570 nm on an ELISA plate reader. Percentage cell survival was expressed as: absorbance treated wells/absorbance of control wells. Each experiment was done in triplicate. IC_{50} values were determined from the compound concentrations that induced a 50% reduction in light absorbance.

Results and discussion

The substituted triazole 1-(2-picolyl)-4-phenyl-1*H*-1,2,3-triazole (**ppt**), recently synthesized *via* "click chemistry" synthetic

protocols,[18,19,24] was used as chelating ligand for Ru(II) complexes with potential antitumor activity.

First of all we tested the reactivity of **ppt** towards two well known Ru(II)-dmso precursors, namely the isomers *trans*- and *cis*-[$RuCl_2(dmso)_4$] (**P1** and **P2**, respectively), in order to verify its preferred binding mode. It is known that treatment of these compounds with neutral *N–N* chelating ligands (*e.g.* 2,2′-bipy) leads mainly to the replacement of two adjacent dmso molecules and to the formation of either *trans*,*cis*-[$RuCl_2$(dmso-S)$_2$(*N–N*)] or *cis*,*cis*-[$RuCl_2$(dmso-S)$_2$(*N–N*)] or to mixtures of the two neutral isomers, depending on the reaction conditions.[39]

We found that treatment of **P1** with an equimolar amount of **ppt** in H_2O at ambient temperature afforded pure *trans*,*cis*-[$RuCl_2$(dmso-S)$_2$(**ppt**)] (**1**) in very good yield. Conversely, a similar synthetic procedure using **P2** as precursor led to the isolation of mixtures of **1** together with its geometrical isomer *cis*,*cis*-[$RuCl_2$(dmso-S)$_2$(**ppt**)] (**2**). Similar mixtures were obtained also upon treatment of either **P1** or **P2** with **ppt** in refluxing water or methanol. However, we observed that the ratio of the two isomers, in *e.g.* methanol, was dependent on the reaction time: whereas at the beginning compound **1** was the predominant species in the reaction mixture, upon increasing the time of reflux the ratio changed in favor of **2**. Thus, consistent with what previously found for similar complexes,[40] compound **1** is the kinetic isomer that isomerizes to the thermodynamically more stable **2** (Scheme 1). Pure compound **2** was isolated in excellent yield when the reaction of **P2** and **ppt** was performed in refluxing ethanol, since the product precipitates spontaneously.

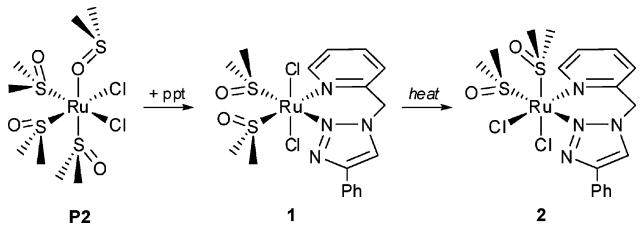

Scheme 1

According to spectroscopic and X-ray evidence (Fig. 3 and Fig. 4; Tables 2 and 3), in **1** and **2** the **ppt** ligand firmly binds to ruthenium in a bidentate fashion - as expected - through the pyridyl

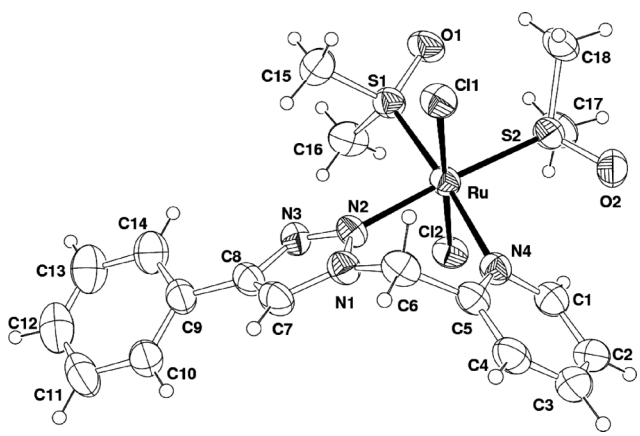

Fig. 3 ORTEP drawing (35% probability ellipsoids) of complex *trans*,*cis*-[$RuCl_2$(dmso-S)$_2$(**ppt**)] (**1**).

Table 2 Selected coordination bond distances (Å) and angles (°) for compounds **1** and **2**

	1	**2**
Ru–N(2)	2.107(4)	2.058(4)
Ru–N(4)	2.172(4)	2.161(4)
Ru–S(1)	2.274(2)	2.276(2)
Ru–S(2)	2.280(2)	2.261(2)
Ru–Cl(1)	2.429(2)	2.437(2)
Ru–Cl(2)	2.397(2)	2.422(2)
N(2)–Ru–N(4)	82.89(16)	87.44(16)
N(2)–Ru–S(1)	93.20(12)	93.45(13)
N(2)–Ru–S(2)	173.94(13)	90.36(14)
N(4)–Ru–S(1)	174.72(12)	175.28(12)
N(4)–Ru–S(2)	91.76(11)	88.95(13)
S(1)–Ru–S(2)	92.31(6)	95.68(7)
N(2)–Ru–Cl(1)	89.44(12)	91.26(14)
N(4)–Ru–Cl(1)	94.43(12)	88.27(12)
S(1)–Ru–Cl(1)	89.07(6)	87.07(6)
S(2)–Ru–Cl(1)	88.13(6)	176.71(6)
N(2)–Ru–Cl(2)	90.05(12)	177.36(13)
N(4)–Ru–Cl(2)	85.26(12)	90.22(11)
S(1)–Ru–Cl(2)	91.20(6)	88.78(6)
S(2)–Ru–Cl(2)	92.35(6)	90.81(7)
Cl(1)–Ru–Cl(2)	179.43(5)	87.44(6)

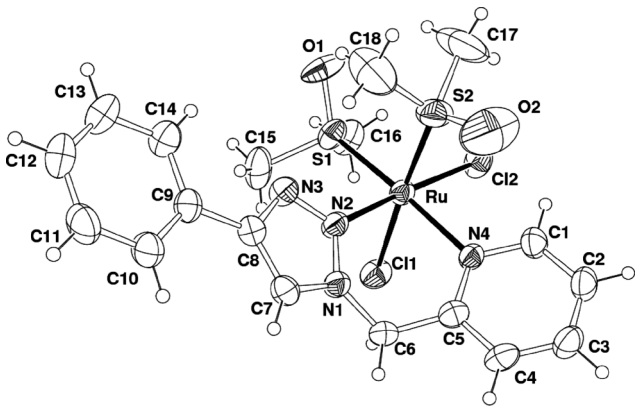

Fig. 4 ORTEP drawing (35% probability ellipsoids) of complex *cis*,*cis*-[$RuCl_2$(dmso-S)$_2$(**ppt**)] (**2**).

nitrogen atom and the triazole N2, thus forming a 6-membered chelate ring. Bound **ppt** adopts a bent conformation, with the CH_2 group that points towards an axial chloride ligand (Cl(1)). The pyridine and triazole rings form a dihedral angle of 56.0(2)° and 42.2(2)° in **1** and **2**, respectively. The Ru–S (range 2.261(2)–2.280(2) Å) and Ru–Cl (2.397(2)–2.437(2) Å) bond distances are comparable with the values observed in other Ru(II)-dmso-Cl complexes.[12,40,41] The Ru–N(2) bond length is significantly longer in **1** than in **2** (2.107(4) *vs.* 2.058(4) Å) due to the different donor atom in *trans* position (dmso-S *vs.* Cl, respectively). In both isomers the Ru–N(4) bond distance, with a mean value of 2.167(4) Å, is longer than Ru–N(2). It is worth noting that in **2** the phenyl ring of **ppt** is almost coplanar with the triazole ring (dihedral angle 3.8(3)°, Table 3) indicating conjugation between them, while the dihedral angle is significantly wider in **1** (28.8(2)°). This latter feature favors a π–π interaction between the phenyl rings and between the pyridyl rings of symmetry related molecules at 3.660(4) and 3.611(4) Å, respectively, that originates a 1D chain (Fig. S1, ESI†).

The IR spectra of the two isomeric complexes **1** and **2** are very similar: beside the bands pertaining to the **ppt** ligand, they show

Table 3 Parameters characterizing the conformational geometry of **ppt** ligand in compounds **1–4**

	1	**2**	**3**	**4**
N(1)–C(6)–C(5)/°	111.6(4)	115.2(5)	112.8(7)	112.7(5)
N(2)–N(1)–C(6)–C(5)/°	−59.3(6)	56.8(7)	−58.6(10)	57.0(8)
N(4)–C(5)–C(6)–N(1)/°	51.3(6)	−50.6(7)	59.7(11)	−60.8(8)
py[a]/triaz[b]/°	56.0(2)	42.2(2)	56.9(4)	48.7(2)
py/equator plane[c]/°	42.9(1)	28.7(1)	32.0(4)	27.1(1)
triaz/equator plane[c]/°	34.2(2)	30.5(1)	34.8(4)	33.9(2)
triaz/phenyl/°	28.8(2)	3.8(3)	40.8(3)	5.5(5)
d C(6)[d]/Å	1.489(7)	1.292(8)	1.32(1)	1.327(9)

[a] mean plane through the pyridine ring. [b] mean plane through the triazole ring. [c] equatorial mean plane through N(2)/N(4)/S(1)/S(2) (in **1**, **3**, **4**) and N(2)/N(4)//S(1)/Cl(2) in **2**. [d] displacement of C(6) from the equatorial plane.

strong bands between 1070 and 1105 cm^{-1} typical of the S═O stretching modes of the dmso-S ligands.

The ^1H NMR spectrum of **1** in $CDCl_3$ (Fig. S2, ESI†) is characterized by the presence of four relatively broad singlets in the region typical for dmso-S (δ = 3.86, 3.64, 3.52 and 3.20) which were attributed to the diastereotopic methyl groups of the two inequivalent dmso-S ligands. The two diastereotopic protons of the CH_2 junction resonate as two broad doublets quite far apart from one another: one doublet falls at 5.26 ppm whereas the other is in the aromatic region (δ = 7.76). The latter resonance is not distinguishable in the ^1H NMR spectrum since it overlaps with that of C4H, but it is clearly evident in the ^1H-^1H COSY spectrum - where it is coupled with the resonance of the geminal proton - and in the ^1H-^{13}C HSQC in which both proton resonances are correlated to the same carbon resonance (Fig. S3, ESI†). The other resonances appear in the aromatic area and are slightly broadened as well. Broadened peaks were observed also in the ^{13}C NMR spectrum, in particular those of the aromatic rings attached to Ru and of the methyl groups of the dmso ligands. Similar spectra were also observed in CD_3NO_2.

The presence of four dmso resonances in the ^1H NMR spectrum of **1** implies that the equatorial plane is not a plane of symmetry for the complex. The broadening of some resonances suggests that a motion - that formally exchanges pairwise methyls on each dmso-S ligand and the diastereotopic CH_2 protons - is occurring at a rate that is relatively slow on the NMR time scale. Most likely this is the flipping motion of the bent ligand that brings the CH_2 junction in two equivalent limiting positions either above or below the equatorial plane. Indeed, the resonances of the exchanged protons become sharp upon lowering the temperature at 273 K, when this motion becomes slow on the NMR time scale (Fig. 5).

In contrast, the ^1H NMR spectrum of complex **2** in $CDCl_3$ at room temperature (Fig. S2, ESI†) displays well resolved sharp peaks for both the **ppt** and the inequivalent dmso-S ligands. It is likely that in **2**, owing to the greater bulkiness of one axial ligand (dmso-S) compared to the other (Cl), the 6-membered **ppt** chelate ring is more rigid and basically maintains in solution the same geometry as that found in the solid state (see above).

Having established that the substituted triazole **ppt** behaves as a typical neutral *N–N* chelating ligand and easily replaces adjacent dmso ligands in Ru-dmso complexes, we investigated its reactivity towards the precursors of Ru-[9]aneS$_3$ half-sandwich coordination compounds.

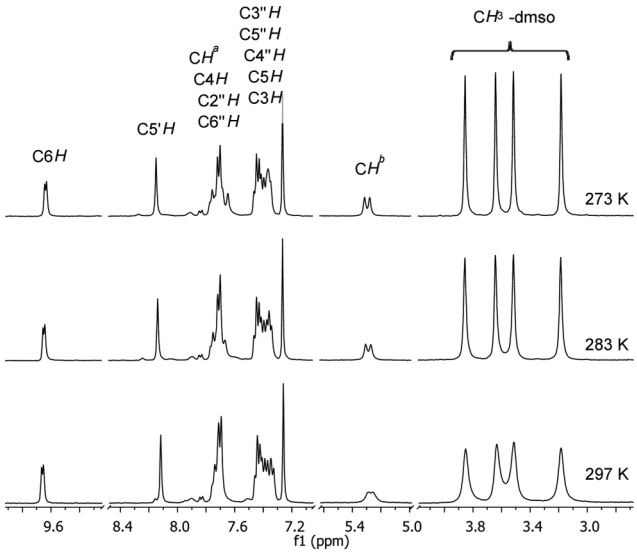

Fig. 5 ^1H NMR spectrum of **1** in $CDCl_3$ at various temperatures.

Treatment of the chloride-free Ru(II) precursor [Ru([9]aneS$_3$)-(dmso)$_3$][CF_3SO_3]$_2$ (**P3**) with an equimolar amount of **ppt** in refluxing methanol afforded the half-sandwich dmso derivative [Ru([9]aneS$_3$)(dmso-S)(**ppt**)][CF_3SO_3]$_2$ (**3**) in good yield. Similarly, treatment of the precursor [Ru([9]aneS$_3$)Cl(dmso-S)$_2$][CF_3SO_3] (**P4**) with **ppt** led to the replacement of the two adjacent dmso ligands and to the formation of the monocationic analogue [Ru([9]aneS$_3$)Cl(**ppt**)][CF_3SO_3] (**4**).

Both compounds were characterized by X-ray structural analysis (Fig. 6 and 7; Tables 3 and 4). In each complex the ruthenium ion displays a distorted octahedral geometry with the tridentate [9]aneS$_3$ ligand occupying three positions in facial geometry and the **ppt** ligand bound with the same bidentate fashion as found in **1** and **2**, thus forming a 6-membered ring. The coordination sphere is completed by a dmso molecule bound through S in **3** or by a chloride anion in **4**. The dihedral angle formed by the pyridine and the triazole rings is similar in the two complexes (*ca.* 53° mean value), whereas a larger difference is found for the angle measured between the triazole and the phenyl ring: 40.8(3)° in **3** and only 5.5(5)° in **4**. In the lattice of **4** this almost

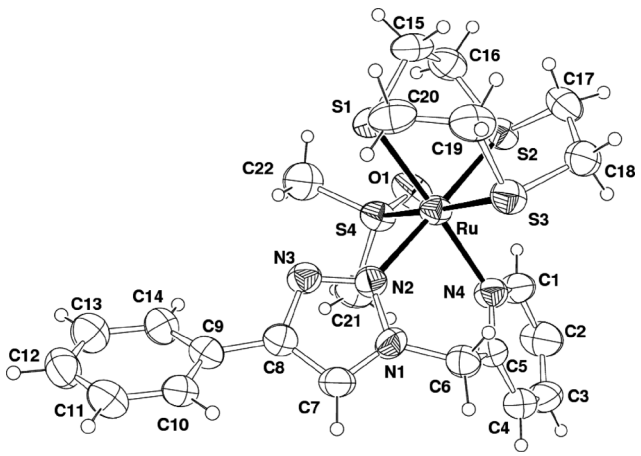

Fig. 6 ORTEP drawing (35% probability ellipsoids) of the complex cation of [Ru([9]aneS$_3$)(dmso-S)(**ppt**)][CF_3SO_3]$_2$ (**3**).

Table 4 Selected coordination bond distances (Å) and angles (°) for compounds **3** and **4**

	3, X = S(4)	**4**, X = Cl(1)
Ru–N(2)	2.108(7)	2.110(5)
Ru–N(4)	2.170(7)	2.152(5)
Ru–S(1)	2.308(2)	2.283(2)
Ru–S(2)	2.326(3)	2.288(2)
Ru–S(3)	2.374(3)	2.280(2)
Ru–X	2.297(3)	2.441(2)
N(2)–Ru–N(4)	85.8(3)	86.3(2)
N(2)–Ru–S(1)	90.97(19)	90.51(15)
N(2)–Ru–S(2)	178.17(19)	178.53(15)
N(2)–Ru–S(3)	95.0(2)	89.93(14)
N(4)–Ru–S(1)	176.5(2)	175.87(15)
N(4)–Ru–S(2)	95.0(2)	94.78(15)
N(4)–Ru–S(3)	91.8(2)	94.07(14)
S(1)–Ru–S(2)	88.27(9)	88.46(7)
S(1)–Ru–S(3)	87.24(9)	88.54(7)
S(2)–Ru–S(3)	86.60(9)	89.00(7)
N(2)–Ru–X	89.8(2)	94.55(14)
N(4)–Ru–X	88.3(2)	88.70(14)
S(1)–Ru–X	92.96(9)	88.94(7)
S(2)–Ru–X	88.54(9)	86.48(7)
S(3)–Ru–X	175.13(9)	174.88(6)

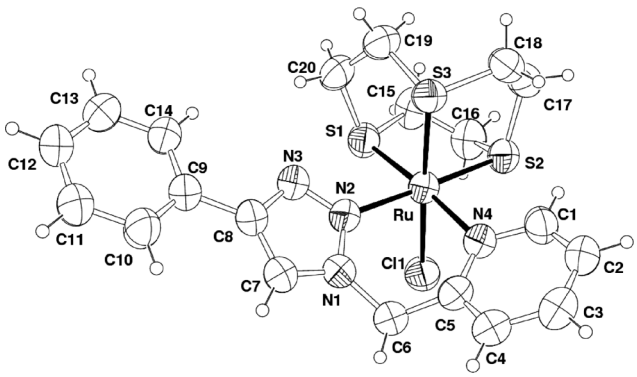

Fig. 7 ORTEP drawing (35% probability ellipsoids) of the complex cation of [Ru([9]aneS$_3$)Cl(**ppt**)][CF$_3$SO$_3$]·H$_2$O (**4**).

flat fragment participates in a double π–π stacking interaction that involves both rings of symmetry related complexes (distance between centroids of 3.567(5) Å, Fig. 8). The Ru–N coordination distances are comparable in the two complexes, while the Ru–S bond distances of [9]aneS$_3$ are slightly longer in **3** (mean of 2.336(3) Å) than in **4** (mean 2.284(2) Å), probably due to the bulkier dmso ligand in **3** compared with chloride in **4**. It is worth noting that the Ru–S([9]aneS$_3$) bond distances in **3** and **4** are slightly shorter (*ca.* 0.05 Å) than in the corresponding precursors [Ru([9]aneS$_3$)(dmso)$_3$]$^{2+}$ (**P3**) and [Ru([9]aneS$_3$)Cl(dmso)$_2$]$^+$ (**P4**).[34] Interestingly, the Ru–Cl and the Ru–N bond lengths in **4** (Table 4) are significantly longer than those found in the corresponding organometallic compound [Ru(η^6-*p*-cymene)Cl(**ppt**)][Cl] (**5**): Ru–Cl = 2.3785(12), Ru–N = 2.082(4) and 2.115(4) Å. This feature suggests the presence of stronger bonds in **5** than in **4**, and it could be relevant for a rationalization of the aquation kinetics (see below).

Complexes **3** and **4** display very similar IR spectra characterized by the presence of bands attributed to the **ppt** ligand and to the CF$_3$SO$_3$ counter ion. In the spectrum of **3** there is an additional

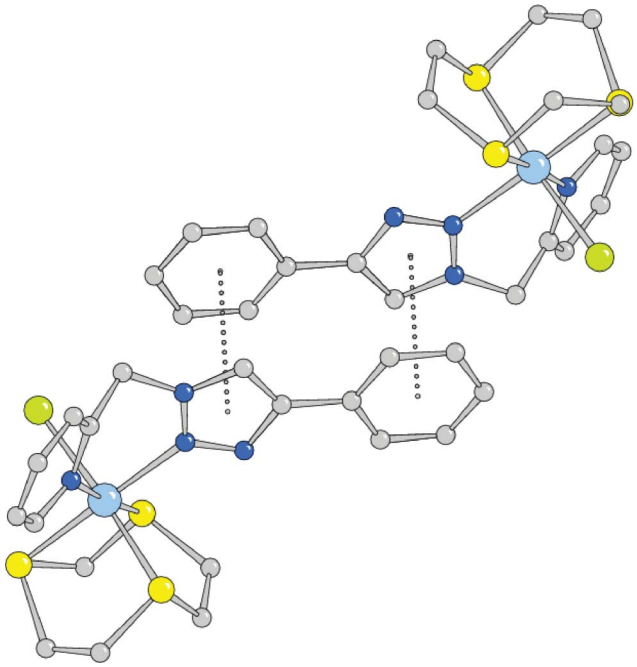

Fig. 8 Crystal packing of compound **4**: pair of complexes arranged about a center of symmetry connected by π–π stacking interactions between phenyl and triazole rings.

strong band at 1099 cm^{-1} attributed to the S=O stretching mode of the dmso-S molecule.

The cationic complexes **3** and **4** undergo slow hydrolysis of the monodentate ligand in aqueous solution, and their ^{1}H NMR spectra in D$_2$O are commented in the next section (see below). The full assignment of the proton and carbon NMR spectra of **3** and **4** was performed by combination of 1D (^{1}H and ^{13}C) and 2D NMR (^{1}H-^{1}H COSY, ^{1}H-^{13}C HSQC and ^{1}H-^{13}C HMBC) experiments in CD$_3$NO$_2$, where both complexes are stable (Fig. S4–S7, ESI†).

The ^{1}H NMR spectrum of **3** in CD$_3$NO$_2$ (Fig. S4, ESI†) is consistent with the molecular structure found in the solid state. The **ppt** ligand displays the typical pattern of resonances in the aromatic region, all downfield shifted compared to the free ligand; the diastereotopic CH$_2$ protons resonate as two well resolved doublets (δ = 6.42 and 6.16) that are coupled to each other in the ^{1}H-^{1}H COSY spectrum and to the same carbon resonance in the ^{1}H-^{13}C HSQC spectrum (Fig. S5 and S6, ESI†). In the upfield region, the methylene groups of [9]aneS$_3$ give a characteristic manifold of partially overlapping multiplets between 2.40 and 3.80 ppm, and the two inequivalent methyl groups of the dmso-S ligand resonate as two well resolved singlets (integrating for 3 H each). Worth noting, while the methyl resonance at δ = 3.57 is in the region typical for dmso-S, the other one (at δ = 1.88) is remarkably shifted upfield because the methyl falls into the shielding cone of the adjacent aromatic rings of **ppt**.[13] The ^{13}C NMR spectrum displays 11 resolved resonances between 125.8 and 158.2 ppm, attributed to the 13 aromatic carbon atoms of the ligand **ppt** (C2″ and C3″ are equivalent to C6″ and C5″, respectively), and 9 resonances in the upfield region assigned to the CH$_2$ group of **ppt** (δ = 54.7), to the two methyl groups of the dmso-S ligand (δ = 45.8 and 41.8) and to the six inequivalent methylene groups of [9]aneS$_3$ (from 37.0 to 28.1 ppm). The assignment of the quaternary carbons (C2,

C4′ and C1″) was achieved by the long range 2D heteronuclear ^{1}H-^{13}C HMBC experiments (Fig. S6, ESI†).

The corresponding chloride complex **4** shows similar ^{1}H and ^{13}C NMR spectra in CD_3NO_2 with the obvious absence of the dmso resonances (Fig. S4 and S7, ESI†).

Chemical behavior in aqueous solution

The chemical behavior of the new water-soluble cationic complexes **3** and **4**, and of the previously described organometallic analogue **5**, was qualitatively investigated by ^{1}H NMR spectroscopy in D_2O at room temperature.

After dissolution in D_2O the ^{1}H NMR spectrum of **3** changed slowly in time due to dmso dissociation: the two dmso-S singlets gradually decreased and were eventually replaced (in *ca.* 24 h) by the resonance of free DMSO at δ = 2.71. The formation of the aqua species [Ru([9]aneS$_3$)(H$_2$O)(**ppt**)]$^{2+}$ (**3a**, Scheme 2) induced observable changes also in the resonances of **ppt** and [9]aneS$_3$; in particular, the two doublets of the methylene group of **ppt** (δ = 6.32 and 6.11) were replaced by two new doublets (δ = 6.40 and 6.00), indicating that the coordination mode of this ligand was unaffected by the aquation process (Fig. 9).

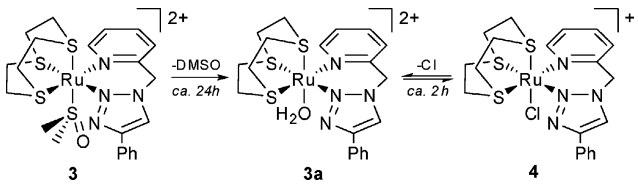

Scheme 2 Chemical behavior of compounds **3** and **4** in aqueous solution.

A remarkably similar behavior, although faster, was observed for **4** in aqueous solution. The hydrolytic process involves the release of the Cl^- ion as indicated by the gradual replacement of the resonances of **4** by those of **3a** (Fig. S8, ESI†). At equilibrium, after *ca.* 2h, the ratio between **4** and **3a** was *ca.* 1 : 5. Addition of 100 mM NaCl in the equilibrated solution reversed the ratio between **4** and **3a** from 1 : 5 to 3 : 1 (within *ca.* 1h, Fig. S9, ESI†).

The chemical behavior of the organometallic compound **5** is similar to that of the corresponding coordination complex **4**. Upon dissolution in D_2O, all the resonances of **5** were slowly replaced by a new set of resonances with similar pattern which were attributed to the aqua species [Ru(η^6-*p*-cymene)(H$_2$O)(**ppt**)]$^{2+}$ (**5a**, Fig. S10, ESI†). After 1 day the ratio between **5** and **5a** was *ca.* 1 : 1 and remained unchanged afterwards. Addition of 100 mM NaCl in the previous solution reversed the equilibrium quantitatively towards the parent compound **5**.

Kinetics of aquation

The kinetics of aquation of compounds **3** and **4** were quantitatively studied by UV-Vis spectroscopy at 25.0 °C on 0.15 mM solutions. For comparison, compound **5** was also studied under the same conditions. The UV-Vis spectra of all compounds show significant time-dependent changes in the region 200–500 nm (Fig. 10, and Fig. S11 and S12 in ESI†) with clean isosbestic points, suggesting the occurrence of a single hydrolytic process (*i.e.* conversion of the parent dmso/Cl complex to the corresponding aqua species) consistent with the NMR observations.

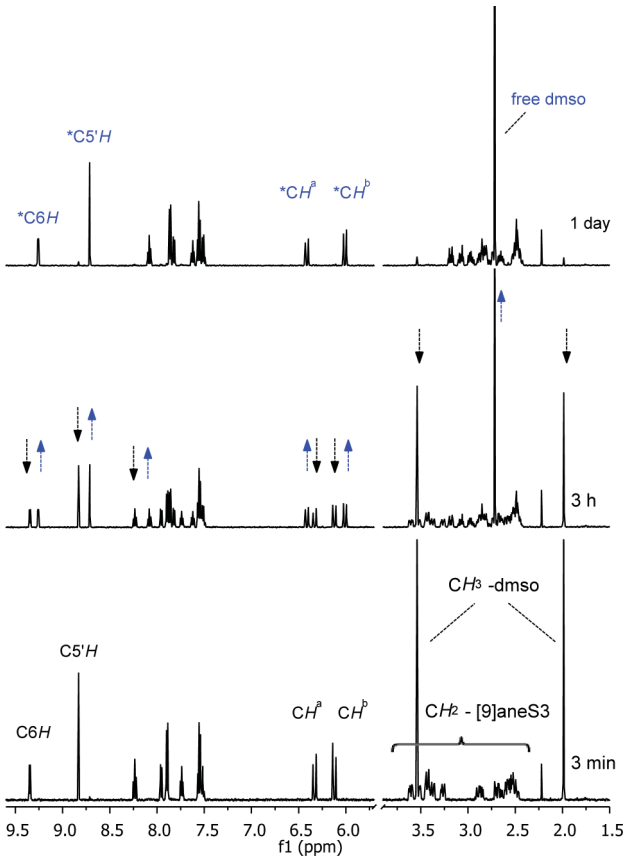

Fig. 9 ^{1}H NMR spectral changes during the aquation of **3** (2.0 mM) in D_2O at 25.0 °C. With (*) are indicated selected resonances of the aquated species **3a** (**3a**: δ_H (500 MHz, D_2O) 9.26 (1 H, d, *J* 4.8, C6*H*), 8.71 (1 H, s, C5′*H*), 8.08 (1 H, td, *J* 7.7, 1.5, C4*H*), 7.86 (2 H, d, *J* 7.0, C2″*H*/C6″*H*), 7.82 (1 H, d, *J* 7.8, C3*H*), 7.62 (1 H, t, *J* 6.7, C5*H*), 7.59–7.53 (2 H, m, C3″*H*/C5″*H*), 7.53–7.48 (1 H, m, C4″*H*), 6.41 (1 H, d, *J* 16.0, C*H*^{a} **ppt**), 6.01 (1 H, d, *J* 16.0, C*H*^{b} **ppt**), 3.22–3.14 (1 H, m, C*H*$_2$ [9]aneS$_3$), 3.12–3.04 (1 H, m, C*H*$_2$ [9]aneS$_3$), 3.01–2.70 (4 H, m, C*H*$_2$ [9]aneS$_3$), 2.70–2.62 (1 H, m, C*H*$_2$ [9]aneS$_3$), 2.55–2.41 (4 H, m, C*H*$_2$ [9]aneS$_3$)).

The wavelength corresponding to the maximum change in absorption was selected for the kinetic studies. In each case the time dependence of the absorbance followed first-order kinetics (Fig. 10), and yielded the rate constants k_{H2O} listed in Table 5. It can be seen that the aquation reaction of the chloride derivative **4** is about 5-fold faster than that of the dmso derivative **3**. In addition, the k_{H2O} values are strongly dependent on the nature of the face-capping ligand: aquation is *ca.* 10 times faster for the coordination half-sandwich complex **4** than for the corresponding

Table 5 Rate constants for the aquation and half-lives at 25.0 °C in H_2O for compounds **3–5**

Compound	λ_{max}[a] [nm]	λ_{min}[a] [nm]	Isosbestic points [nm]	k_{H2O} [10^{-5} s^{-1}]	$(t_{1/2})_{H2O}$ [min]
3	319	**266**, 289	297	8.43 ± 0.01	137.2 ± 0.2
4	273	**337**, 411	240, 302	40.27 ± 0.01	28.7 ± 0.01
5	243	213, **273**	233, 253	4.10 ± 0.04	281.9 ± 2.7

[a] Wavelengths obtained from the time evolution difference electronic absorption spectra. In bold are indicated the wavelengths selected for the kinetic studies.

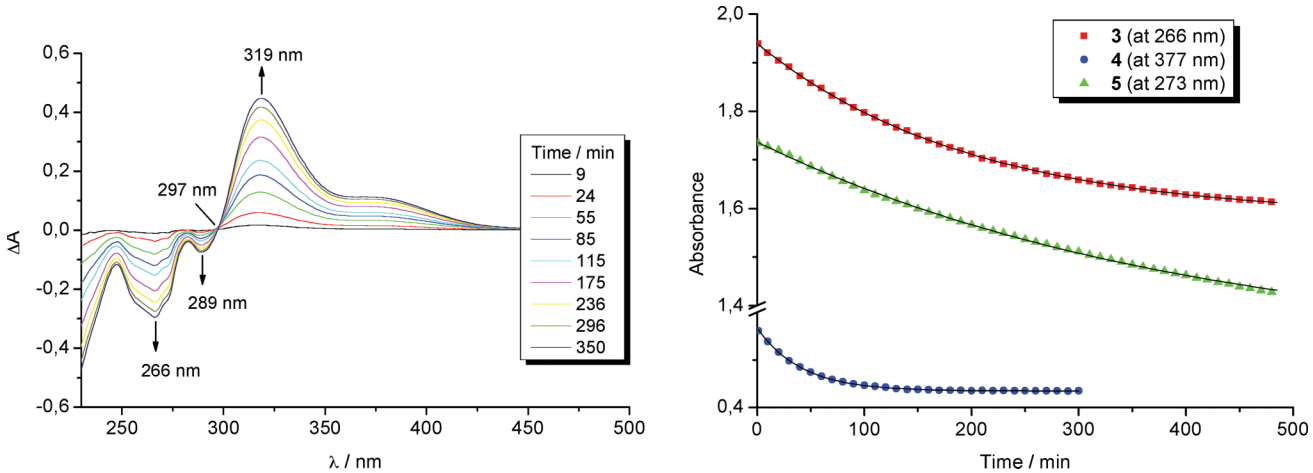

Fig. 10 Left: Time evolution of UV-Vis difference spectra during the aquation of complex **3** ($\Delta A = A_t - A_0$, where A_t = absorbance at time t and A_0 = absorbance at $t = 2$ min (*i.e.* the time at which the first spectrum was recorded)); Right: Time-dependence of the absorbance at selected wavelengths for the aquation of the complexes **3–5** in H_2O at 25.0 °C (Full lines represent computer fits giving the first-order rate constants for the aquation, listed in Table 5).

Table 6 Cytotoxic activity expressed as IC_{50} (μM ± SD) of all tested compounds at 48 h and 72 h on the human cancer cell lines HEp-2 and A-549

	IC_{50}, μM ± SD			
	HEp-2		A-549	
Compound	48h	72h	48h	72h
ppt	150 ± 19	150 ± 16	100 ± 32	100 ± 8
3	280 ± 18	> 300	> 300	> 300
P3	> 300	> 300	100 ± 6	250 ± 13
4	> 300	> 300	60 ± 17	80 ± 3
5	> 300	> 300	200 ± 16	125 ± 6
P5	94 ± 9	100 ± 14	170 ± 12	210 ± 12
Cisplatin	7.5 ± 11	80 ± 10	200 ± 7	105 ± 10

organometallic compound **5**. The aquation process is also more pronounced for **4** than for **5**. These observations are in agreement with the finding that, in solid state, the Ru–Cl bond is weaker in **4** than in **5**.

In vitro experiments

The cytotoxic effects of compounds **3–5** were evaluated after 48 and 72 h of exposure on two human cancer cell lines: the cisplatin-sensitive human larynx carcinoma cell line (HEp-2) and the cisplatin-resistant human alveolar squamous carcinoma epithelial cells (A-549).[42] The tested compounds exhibited cytotoxic effects that enabled the construction of concentration-response curves and calculation of the IC_{50} values (Table 6).

The results show that, in general, the antiproliferative activity of the tested ruthenium compounds is lower than that of cisplatin and basically they are not cytotoxic against the specific cells. Often the activity of **ppt** or of the precursors is higher than that of the half-sandwich derivatives. Notable exception is compound **4** that, on the A-549 cell line shows an IC_{50} value almost one-order of magnitude lower than that of cisplatin. Conversely, **4** does not show any activity on HEp-2 cells, indicating a remarkable selectivity towards the cisplatin-resistant cell line.

In contrast to chloride-derivative **4**, the dmso-derivative **3** exhibits no activity towards both tested cell lines indicating that the leaving group, and as consequence the aquation rate, plays an important role on the activity of such complexes.

Conclusions

We described here the preparation and structural characterization, mainly by NMR spectroscopy in solution and by X-ray crystallography in the solid state, of four new Ru(II) complexes bearing a 1,4-disubstituted 1,2,3-triazole, *i.e.* 1-(2-picolyl)-4-phenyl-1*H*-1,2,3-triazole (**ppt**) as chelating ligand: two isomeric neutral Ru-dmso complexes, *trans*,*cis*-[$RuCl_2$(dmso-S)$_2$(**ppt**)] (**1**) and *cis*,*cis*-[$RuCl_2$(dmso-S)$_2$(**ppt**)] (**2**), and two half-sandwich Ru-[9]aneS$_3$ coordination compounds, [Ru([9]aneS$_3$)(dmso-S)(**ppt**)][CF_3SO_3]$_2$ (**3**) and [Ru([9]aneS$_3$)Cl(**ppt**)][CF_3SO_3] (**4**). In all four compounds **ppt** is bound to Ru through the N2 of the azole ring and the pyridyl nitrogen atom forming a stable 6-membered ring. The original aim of this work was to evaluate the preferential binding mode of **ppt** on octahedral Ru complexes and to assess how it influences the antiproliferative activity of half-sandwich Ru coordination compounds, thus developing further the structure–activity relationship investigation in this series of structurally similar compounds.

The two neutral Ru-dmso complexes **1** and **2** are insoluble in water, and therefore no further biological investigation was performed. On the other hand, the cationic half-sandwich complexes **3** and **4** are fairly soluble in water. Hence, in view of their potential antitumor activity, their chemical behavior in aqueous solution was studied by UV-Vis and NMR spectroscopy and compared to that of the previously described organometallic analogue [Ru(η^6-*p*-cymene)Cl(**ppt**)][Cl] (**5**). We found that the aquation rate of such complexes, and consequently their potential biological activity, depends on the nature of the face-capping ligand (Cl is released faster from the coordination compound **4** than from the organometallic analogue **5**) and of the leaving group (Cl > dmso-S). Compounds **3–5** were tested also *in vitro* for antiproliferative activity against two human cancer cell lines in comparison with

the precursors $[Ru([9]aneS_3)(dmso)_3][CF_3SO_3]_2$ (**P3**) and $[RuCl(\mu\text{-}Cl)(\eta^6\text{-}p\text{-cymene})]_2$ (**P5**), the free ligand (**ppt**) and cisplatin. All tested compounds were found to be less cytotoxic than cisplatin with the exception of **4**, the compound that hydrolyses fastest, against cisplatin-resistant human lung squamose carcinoma cells (A-549). The selective cytotoxic activity found for **4** against A-549 cells is particularly interesting: lung cancer is the most common cause of cancer-related death and squamous cell carcinoma is the second most common type of lung cancer.

So far, only half-sandwich Ru-$[9]aneS_3$ complexes capable of hydrolyzing the monodentate ligand at a reasonable rate and of acting as hydrogen bond donors through the chelating ligand, like $[Ru([9]aneS_3)Cl(en)][CF_3SO_3]$ and $[Ru([9]aneS_3)Cl(dach)][PF_6]$ (where dach = 1,2-diaminocyclohexane), were found to have some antiproliferative activity *in vitro*.[12,13,15] However, these compounds were less active compared to their organometallic analogues. Here we show that the nature of the face-capping ligand is not the most important feature for activity: the cytotoxicity of the organometallic compound **5** towards the two tested cancer cell lines is comparable or lower than that of the analogous coordination compound **4**. Most likely the rate of aquation plays an important role in differentiating these two structurally similar compounds. In addition, we showed here that introduction of a chelating ligand that is unable of making hydrogen bonds, such as **ppt**, not necessarily induces the total loss of antiproliferative activity. Possibly, also the nature of the pendant group in position 4 influences the activity. For example, the phenyl ring in **ppt** is expected to impart hydrophobicity to the complex that improves its membrane permeability, and might be involved in additional stacking interaction (*e.g.* intercalation) with DNA bases. In the future, we aim to prepare by click reaction new 1-(2-picolyl)-1,2,3-triazole ligands bearing more advanced pendant functional groups in position 4 that might improve the properties of their half-sandwich complexes.

The compounds described in this manuscript, despite their limited cytotoxic properties *in vitro*, may hold promise for therapeutic purposes *in vivo*. Indeed, the Ru(III) compound NAMI-A, that is currently being tested on patients in a phase 1–2 study, was found to be poorly cytotoxic *in vitro* but has an effect on metastasis formation *in vivo*. Nowadays, it is becoming increasingly evident that the classical cytotoxicity tests are often insufficient models for drug screening, since they lack essential components of the *in vivo* environment, such as the extracellular matrix components (ECM). In this respect, some organo-ruthenium half-sandwich complexes belonging to the so-called RAPTA family developed by the group of Dyson,[43] although poorly toxic in classical proliferation assays (probably because they interact with ECM components),[44,45] were found to be effective against metastasis formation and as inhibitors of cell invasion pathways. Therefore, in this context, our new complexes might be of interest for further evaluation in biological systems.

Acknowledgements

This work was performed within the framework of COST Action D39. The group of Trieste gratefully acknowledges Regione FVG (Project "Nuove Terapie e Farmaci Antitumorali"), Fondazione CRTrieste, Fondo Trieste, Fondazione Beneficentia Stiftung for financial support and BASF Italia Srl for a generous donation of hydrated ruthenium chloride. Fondazione CRTrieste is also gratefully acknowledged for the munificent donation of a Varian 500 NMR spectrometer to the Department of Chemical Sciences. Financial support from the Slovenian Research Agency (ARRS) through projects J1-0200-0103-008, P1-0230-0103 and EN→FIST Centre of Excellence, Dunajska 156, SI-1000 Ljubljana is gratefully acknowledged. We thank Dr A. Bergamo (Callerio Foundation Onlus, Trieste, Italy) for her critical comments on the manuscript, as well as Dr Radostina Alexandrova (Bulgarian Academy of Sciences, Sofia, Bulgaria) for her contribution to the biological experiments.

References

1 A. Levina, A. Mitra and P. A. Lay, *Metallomics*, 2009, **1**, 458–470.
2 I. Bratsos, T. Gianferrara, E. Alessio, C. G. Hartinger, M. A. Jakupec and B. K. Keppler, in *Bioinorganic Medicinal Chemistry*, ed. E. Alessio, Wiley-VCH, Weinheim, 2011, pp. 151–174.
3 J. M. Rademaker-Lakhai, D. van den Bongard, D. Pluim, J. H. Beijnen and J. H. M. Schellens, *Clin. Cancer Res.*, 2004, **10**, 3717–3727.
4 C. G. Hartinger, S. Zorbas-Seifried, M. A. Jakupec, B. Kynast, H. Zorbas and B. K. Keppler, *J. Inorg. Biochem.*, 2006, **100**, 891–904.
5 I. Bratsos, S. Jedner, T. Gianferrara and E. Alessio, *Chimia*, 2007, **61**, 692–697.
6 C. G. Hartinger, M. A. Jakupec, S. Zorbas-Seifried, M. Groessl, A. Egger, W. Berger, H. Zorbas, P. J. Dyson and B. K. Keppler, *Chem. Biodiversity*, 2008, **5**, 2140–2155.
7 G. Süss-Fink, *Dalton Trans.*, 2010, **39**, 1673–1688.
8 Y. K. Yan, M. Melchart, A. Habtemariam and P. J. Sadler, *Chem. Commun.*, 2005, 4764–4776.
9 S. J. Dougan and P. J. Sadler, *Chimia*, 2007, **61**, 704–715.
10 R. E. Aird, J. Cummings, A. A. Ritchie, M. Muir, R. E. Morris, H. Chen, P. J. Sadler and D. I. Jodrell, *Br. J. Cancer*, 2002, **86**, 1652–1657.
11 A. Habtemariam, M. Melchart, R. Fernández, S. Parsons, I. D. H. Oswald, A. Parkin, F. P. A. Fabbiani, J. E. Davidson, A. Dawson, R. E. Aird, D. I. Jodrell and P. J. Sadler, *J. Med. Chem.*, 2006, **49**, 6858–6868.
12 B. Serli, E. Zangrando, T. Gianferrara, C. Scolaro, P. J. Dyson, A. Bergamo and E. Alessio, *Eur. J. Inorg. Chem.*, 2005, 3423–3434.
13 I. Bratsos, S. Jedner, A. Bergamo, G. Sava, T. Gianferrara, E. Zangrando and E. Alessio, *J. Inorg. Biochem.*, 2008, **102**, 1120–1133.
14 I. Bratsos, G. Birarda, S. Jedner, E. Zangrando and E. Alessio, *Dalton Trans.*, 2007, 4048–4058.
15 I. Bratsos, E. Mitri, E. Zangrando, A. Bergamo, G. Sava and E. Alessio, *unpublished results*.
16 T. Gianferrara, A. Bergamo, I. Bratsos, B. Milani, C. Spagnul, G. Sava and E. Alessio, *J. Med. Chem.*, 2010, **53**, 4678–4690.
17 M. Meldal and C. W. Tornøe, *Chem. Rev.*, 2008, **108**, 2952–3015.
18 V. V. Rostovtsev, L. G. Green, V. V. Fokin and K. B. Sharpless, *Angew. Chem., Int. Ed.*, 2002, **41**, 2596–2599.
19 C. W. Tornøe, C. Christensen and M. Meldal, *J. Org. Chem.*, 2002, **67**, 3057–3064.
20 A. Bastero, D. Font and M. A. Pericàs, *J. Org. Chem.*, 2007, **72**, 2460–2468.
21 T. L. Mindt, H. Struthers, L. Brans, T. Anguelov, C. Schweinsberg, V. Maes, D. Tourwé and R. Schibli, *J. Am. Chem. Soc.*, 2006, **128**, 15096–15097.
22 H. Struthers, T. L. Mindt and R. Schibli, *Dalton Trans.*, 2010, **39**, 675–696.
23 A. Maisonial, P. Serafin, M. Traïkia, E. Debiton, V. Théry, D. J. Aitken, P. Lemoine, B. Viossat and A. Gautier, *Eur. J. Inorg. Chem.*, 2008, 298–305.
24 D. Urankar, B. Pinter, A. Pevec, F. De Proft, I. Turel and J. Košmrlj, *Inorg. Chem.*, 2010, **49**, 4820–4829.
25 S.-Q. Bai, S. Leelasubcharoen, X. Chen, L. L. Koh, J.-L. Zuo and T. S. A. Hor, *Cryst. Growth Des.*, 2010, **10**, 1715–1720.
26 W. S. Brotherton, H. A. Michaels, J. Tyler Simmons, R. J. Clark, N. S. Dalai and L. Zhu, *Org. Lett.*, 2009, **11**, 4954–4957.
27 J. D. Crowley and P. H. Bandeen, *Dalton Trans.*, 2010, **39**, 612–623.
28 J. D. Crowley, P. H. Bandeen and L. R. Hanton, *Polyhedron*, 2010, **29**, 70–83.

29 Y. Fu, Y. Liu, C. Zhong, H. Li, X. G. Chen and J. G. Qin, *Chin. J. Inorg. Chem.*, 2010, **26**, 1133–1140.
30 K. J. Kilpin and J. D. Crowley, *Polyhedron*, 2010, **29**, 3111–3117.
31 G.-C. Kuang, H. A. Michaels, J. T. Simmons, R. J. Clark and L. Zhu, *J. Org. Chem.*, 2010, **75**, 6540–6548.
32 D. Urankar, A. Pevec, I. Turel and J. Košmrlj, *Cryst. Growth Des.*, 2010, **10**, 4920–4927.
33 I. Bratsos and E. Alessio, *Inorg. Synth.*, 2010, **35**, 148–152.
34 E. Iengo, E. Zangrando, E. Baiutti, F. Munini and E. Alessio, *Eur. J. Inorg. Chem.*, 2005, 1019–1031.
35 Z. Otwinowski and W. Minor, *Methods Enzymol.*, 1997, **276**, 307–326.
36 G. M. Sheldrick, *SHELXL-97 Programs for Crystal Structure Analysis (Release 97-2)*, University of Göttingen, Germany, 1998.
37 L. J. Farrugia, *J. Appl. Crystallogr.*, 1999, **32**, 837–838.
38 T. Mosmann, *J. Immunol. Methods*, 1983, **65**, 55–63.
39 E. Alessio, *Chem. Rev.*, 2004, **104**, 4203–4242.
40 E. Alessio, E. Iengo, E. Zangrando, S. Geremia, P. A. Marzilli and M. Calligaris, *Eur. J. Inorg. Chem.*, 2000, 2207–2219.
41 M. Calligaris, *Coord. Chem. Rev.*, 2004, **248**, 351–375.
42 P. Zhang, W. Y. Gao, S. Turner and B. S. Ducatman, *Mol. Cancer*, 2003, **2**, 1.
43 P. J. Dyson, *Chimia*, 2007, **61**, 698–703.
44 A. Bergamo, A. Masi, P. J. Dyson and G. Sava, *Int. J. Oncol.*, 2008, **33**, 1281–1289.
45 A. Casini, C. Gabbiani, F. Sorrentino, M. P. Rigobello, A. Bindoli, T. J. Geldbach, A. Marrone, N. Re, C. G. Hartinger, P. J. Dyson and L. Messori, *J. Med. Chem.*, 2008, **51**, 6773–6781.